

Polarization-modulated population distribution of nitrogen molecular ions in a strong laser fieldYewei Chen,^{1,2} Chaohui Zhou,¹ Xu Lu^{ⓧ,2,3}, Liang Xu^{ⓧ,1,*}, Qi Yuan^{ⓧ,1}, Siyi He,^{2,3} Rongyu Gong,^{1,2} Ning Zhang,^{2,3} Quanjun Wang^{ⓧ,2}, Shunlin Huang^{ⓧ,2}, Yuzhu Wu,^{2,4} Yi Liu^{ⓧ,1,†} and Jinping Yao^{ⓧ,2,‡}¹*School of Optical-Electrical and Computer Engineering, University of Shanghai for Science and Technology, Shanghai 200093, China*²*State Key Laboratory of High Field Laser Physics, Shanghai Institute of Optics and Fine Mechanics, Chinese Academy of Sciences, Shanghai 201800, China*³*Center of Materials Science and Optoelectronics Engineering, University of Chinese Academy of Sciences, Beijing 100049, China*⁴*School of Microelectronics, Shanghai University, Shanghai 200444, China*

(Received 22 January 2024; accepted 19 April 2024; published 20 May 2024)

We investigate the dependence of N_2^+ lasing radiation on the polarization ellipticity of the pump laser with the 900- and 980-nm wavelengths. Our results show that the 391-nm lasing radiation is stronger with the elliptically polarized laser in the 900-nm pumping case, while the lasing signal decays monotonically with the increasing ellipticity in the 980-nm pumping case. In contrast, the strongest 428-nm lasing appears with the linear polarization laser for both pumping cases. The theoretical simulations reproduce key observations and reveal that the physical origin underlying the ellipticity-dependent behaviors is the sensitivity of photoexcitation of different channels on the wavelength and polarization of the pump laser. At the 900-nm pump wavelength, one-photon excitation from $X^2\Sigma_g^+$ to $A^2\Pi_u$ of N_2^+ plays a dominant role in the population inversion. The elliptically polarized laser is beneficial to the perpendicular transition between the two states. In the 980-nm pumping case, the three-photon excitation from $X^2\Sigma_g^+$ to $B^2\Sigma_u^+$, which prefers linear polarization pumping, dominates the population inversion. The 428-nm lasing gain mainly depends on the population on the $B^2\Sigma_u^+$ state, thus the strongest radiation always occurs in the case of linear polarization. The polarization-dependent behaviors of N_2^+ lasing reflect the complex population inversion mechanism in the strong-field-prepared ionic system.

DOI: [10.1103/PhysRevA.109.053522](https://doi.org/10.1103/PhysRevA.109.053522)**I. INTRODUCTION**

Photoionization is one of the most fundamental processes of the intense laser-matter interaction [1]. When atoms or molecules are exposed to a strong laser field, they will undergo ionization through simultaneously absorbing a lot of photons [2]. Alternatively, the electron wave packet also has some probability to pass through the potential barrier distorted by the laser field, that is, tunneling ionization [1]. No matter whether multiphoton or tunneling ionization plays a dominant role, the electrons lying in inner molecular orbitals, which are more strongly bound to the nucleus, are more difficult to be removed than the outermost electrons [1,3]. As a result, ions produced from strong-field ionization should mainly populate on the ground state rather than excited states. However, generation of N_2^+ lasing [4–6] cannot be well understood by this commonly accepted ionization picture. Previous studies [7–13] show that along with the N_2^+ lasing radiation, the optical gain can be established in the nitrogen gas plasma. According to common laser principle, it means that after the laser pulse is over, the produced ions prefer to stay on the excited states rather than the ground one. Therefore, the discovery of N_2^+ lasing promotes us to revisit the fundamental process of

strong-field ionization and subsequent population distribution on various ionic states.

Various mechanisms have been proposed in the past decade to explain the gain behaviors of N_2^+ lasing, including the laser-ion coupling [8,9,14–16], lasing without inversion [17–19], and electron recollision excitation [20,21], etc. Although the physical mechanism of air lasing is still under debate, the crucial contribution of resonant excitation and electronic coherence has been verified by numerous experimental and theoretical studies [8,9,13,14,19,22–28]. Particularly, the resonance of the laser field with the ionic states following tunnel ionization will give rise to population redistribution on ionic states. The strength of laser-ion coupling depends on the laser parameters; it is thus possible to control the ionic population and then realize a dramatic enhancement of N_2^+ lasing by adjusting the wavelength or polarization of the pump laser. In 2016, Yao *et al.* uncovered the important role of the pump wavelength in the population inversion [8]. In 2019, the 391-nm lasing was enhanced by 2–3 orders of magnitude via modulating the polarization of the pump laser [22] or utilizing the two-color pumping scheme [23]. The combination of two strategies result in the 5–6 orders of magnitude enhancement of N_2^+ lasing [24]. Besides, the influence of the ellipticity of the pump laser on N_2^+ lasing has been investigated intensively since 2013 [20,29–33]. It is found that the stronger N_2^+ lasing can be achieved by using an elliptically polarized driver laser, indicating the possibility to modulate ionic population by changing the laser ellipticity.

*liangxu2021@usst.edu.cn

†yi.liu@usst.edu.cn

‡jinpjngmrg@163.com

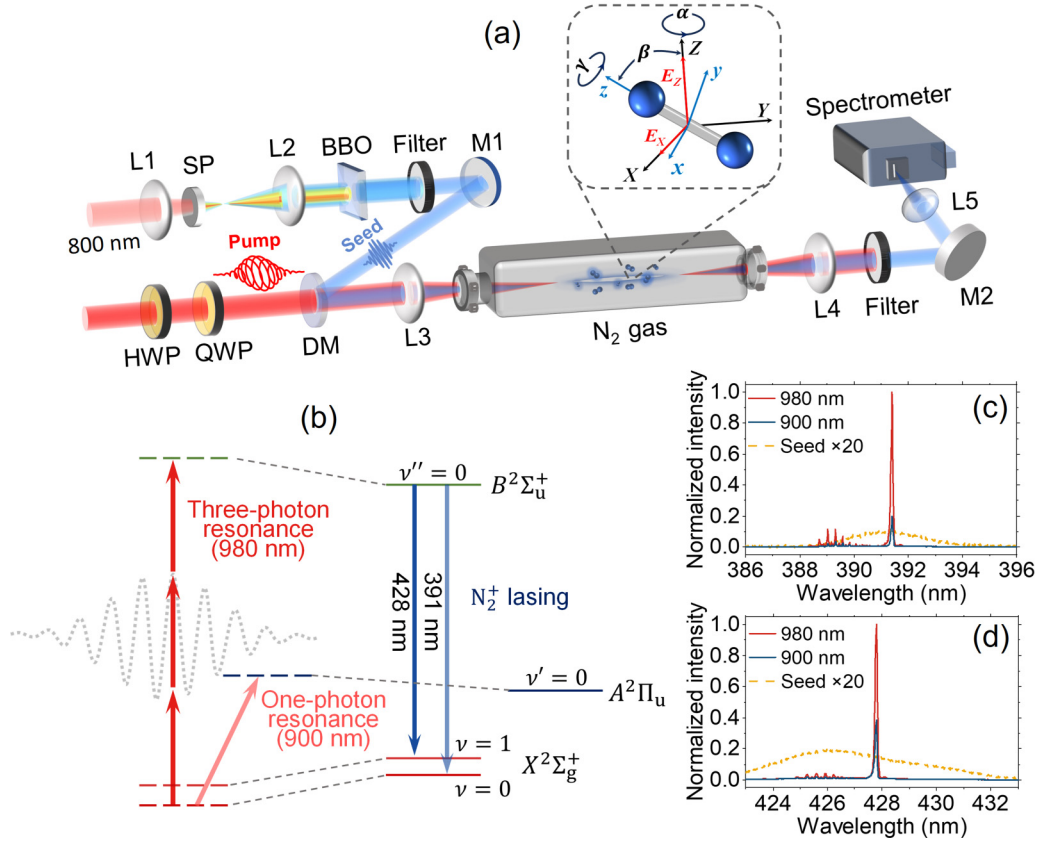


FIG. 1. (a) Schematic of experimental setup. M1, M2: reflective mirror; HWP: half-wave plate; QWP: quarter-wave plate; L1: $f = 20$ -cm lens; L2, L3, L5: $f = 10$ -cm lens; L4: $f = 15$ -cm lens; DM: dichroic mirror; SP: sapphire plate; BBO: beta barium borate. The inset shows the Euler angles (α , β , γ) and pump field components. The transformation between the space- and molecule-fixed coordinates is accomplished by a series of rotation operations with the Euler angles. (b) Schematic illustration of photoexcitation assisted by the ac Stark effect in the two pumping cases and N_2^+ lasing radiation. The solid colored lines represent the field-free eigenstates after the laser field finishes, and the dashed colored lines represent the field-dressed states within the laser field. The typical emission spectra of 391- and 428-nm lasing radiations for the 900- and 980-nm pumping cases are presented in (c) and (d), respectively. The pump and seed pulses were linearly polarized, and their polarization directions were parallel to each other.

More importantly, the ellipticity dependence of lasing radiation also helps us clarify its intriguing gain mechanism to some extent [31–33]. However, most experiments on the ellipticity dependence of N_2^+ lasing are carried out by the 800-nm pump laser. Other pump wavelengths are rarely explored.

In this article, the dependences of 391- and 428-nm lasing signals on the ellipticity of the pump laser were comparatively studied by using the 900- and 980-nm pump lasers. The two pump wavelengths are selected based on the following considerations. First, our recent study indicates that the N_2^+ lasing is significantly enhanced near 1000 nm due to the dynamic three-photon resonance [34], which is different from the 900- and 800-nm pumping cases. Second, the 900- and 980-nm pump lasers have similar spatial profiles and pulse duration. It ensures that the influence of other parameters is minimized when the pump laser wavelength is changed. Thus, the comparative study allows us to examine the influence of excitation mechanism on the ellipticity dependence of N_2^+ lasing, and further uncover the sensitivity of the photoexcitation to the pump laser parameters. The experimental results show that the N_2^+ lasing at 391 nm produced by the two pump wavelengths shows different dependencies on the ellipticity, while similar ellipticity dependence is observed for the 428-nm lasing

signal. The numerical simulations reproduce key experimental observations. The combined experimental and theoretical study reveals individual contributions of single-photon and three-photon resonance to the population inversion in the two pumping cases. This work not only facilitates the understanding for physical mechanism of air lasing, but also offers a route for optimization and manipulation of N_2^+ lasing radiation.

II. EXPERIMENTAL SETUP

The experiment was conducted with the pump-seed scheme, as shown in Fig. 1(a). A laser pulse from the Ti:sapphire laser (Legend Elite-Duo, Coherent Inc.) was split into two beams. One beam with $\sim 95\%$ energy was used to pump the optical parametric amplifier (OPA) (HE-TOPAS, Light Conversion Ltd.), while the other one is used to generate a seed laser. The pump laser was achieved through the frequency doubling of the idler beam from the OPA. Here, we choose two pump lasers with the central wavelength of 900 and 980 nm to study the ellipticity dependence of N_2^+ lasing. The energies of the 900- and 980-nm laser pulses are chosen as 235 and 250 μJ , respectively, which ensures the compa-

rable focused intensity of two pump lasers by considering their slight differences in the pulse duration and focal spot. The combination of a half-wave plate (HWP) and a quarter-wave plate (QWP) was used to change the ellipticity of the pump laser while fixing the major axis. The external seed was generated by the following method. First, the 800-nm femtosecond laser was focused by an $f = 20$ cm lens (L1) and then collimated by an $f = 10$ cm lens (L2). A sapphire plate (SP) was inserted near the focus to induce supercontinuum radiation, and then the supercontinuum signal was frequency doubled with a beta barium borate (BBO) crystal. The 391- and 428-nm seed pulses were obtained by adjusting the phase-matched angle and using the corresponding narrow-band filters. A variable attenuation was inserted in the seed path in order to ensure a comparable intensity at the two seed wavelengths.

The pump and seed pulses were collinearly combined by using a dichroic mirror (DM) and then focused by an $f = 10$ cm lens (L3) into the nitrogen gas chamber. The nitrogen pressure was fixed at 50 mbar and 100 mbar to obtain efficient seed amplification at 391 and 428 nm, respectively. The time delay between the pump and the seed was individually optimized to generate the strongest lasing signal at both 391 and 428 nm, which also enables us to eliminate the influence caused by tuning the angle of the BBO crystal. The generated N_2^+ lasing radiation was separated from the pump pulse by a piece of blue glass filter (FGB37-A), and then was collected into a spectrometer (Shamrock 500i, Andor). The 2400 grooves/mm grating was used for fine spectral analysis, while the 300 grooves/mm grating was adopted for the investigation on the ellipticity dependence to minimize the sensitivity of the spectrometer to polarization.

III. THEORETICAL MODEL

To understand the physical mechanism behind experimental results, we performed the numerical simulations for population dynamics in N_2^+ based on the Bloch equations [14,23,35]. Our theoretical model contains N_2 ionization and sequential N_2^+ excitation between three lowest electronic levels $X^2\Sigma_g^+$, $A^2\Pi_u$, and $B^2\Sigma_u^+$ (abbreviated as X , A , B), which is described by

$$\frac{d\rho}{dt} = -i[H, \rho] + W. \quad (1)$$

Here, ρ , H , and W are the density matrix, Hermitian Hamiltonian, and instantaneous ionization injection, respectively. The diagonal elements in H denote the electronic-vibrational eigenenergies [36]. The nondiagonal ones depict the interaction between N_2^+ and the light field and $H_{vv''}^{XB} = -\mu_{vv''}^{XB} E_z(t)$ is responsible for the X - B parallel transition. Hartree atomic units are used throughout the paper unless stated otherwise. Since the $A^2\Pi_u$ state is doubly degenerate, $E_x(t)$ and $E_y(t)$ couple correspondingly $A^2\Pi_x$ and $A^2\Pi_y$ states via perpendicular transitions, whose Hamiltonians are $H_{vv''}^{XA_x} = -\mu_{vv''}^{XA} E_x(t)$ and $H_{vv''}^{XA_y} = -\mu_{vv''}^{XA} E_y(t)$, respectively. $\mu_{vv''}^{XA}$ and $\mu_{vv''}^{XB}$ are vibration-resolved transition dipole moments with the vibrational quantum number v . The angle-dependent ionization rate $W[\theta(t), \mathbf{E}(t)]$ is a diagonal term and evaluated by the molecular Ammosov-Delone-Krainov

theory [3,37]. $\theta(t)$ is the instantaneous intersection angle between molecular axis and the laser electric field $\mathbf{E}(t)$. The time-dependent electric-field vector $\mathbf{E}(t)$ respectively corresponds to three components $E_x(t)$, $E_y(t)$, and $E_z(t)$ in the molecular coordinate system and $E_X(t)$, $E_Y(t)$, and $E_Z(t)$ in the space coordinate system, which are connected via a rotation matrix with Euler angles (α, β, γ) parameters, as illustrated in the inset of Fig. 1(a). Here 15 levels are included, that is, $X(v = 0-4)$, $A(v' = 0-4)$, and $B(v'' = 0-4)$. Thus, ρ , H , and W are all 15 factorial square matrixes. Other electronic excited states are neglected because of their large transition energies.

In our model, the elliptical polarization laser field is defined in a X - Z plane in the space coordinate system. It is expressed as

$$\begin{aligned} \mathbf{E}(t) &= \mathbf{E}_Z(t) + \mathbf{E}_X(t) \\ &= E_0 \cos\Theta f\left(t - \frac{T_d}{2}\right) \mathbf{e}_Z + E_0 \sin\Theta f\left(t + \frac{T_d}{2}\right) \mathbf{e}_X \end{aligned} \quad (2)$$

where E_0 , $f(t)$, and T_d signify the amplitude, envelope, and time delay of the two components of the elliptically polarized laser field, respectively. $E_0 = \sqrt{I_0}/(3.51 \times 10^{16})$ and the unit of I_0 is W/cm^2 . $f(t) = \exp[-2\ln 2(t^2/\tau^2)]\sin(\omega t)$, and $\tau = 60$ fs and ω denote the full width at half maximum of the pulse duration and the carrier frequency, respectively. Two wavelengths are selected according to the experiment, 900 nm ($\omega = 0.05065$ a.u.) and 980 nm ($\omega = 0.04652$ a.u.). T_d is fixed as $0.5\pi/\omega$, corresponding to the phase delay of a quarter cycle. Θ is adjusted in the range from $-\pi/4$ to $\pi/4$ to control the laser ellipticity which is defined as $\xi = \tan\Theta$, and $\Theta = -\pi/4$ or $\pi/4$ corresponds to the circular polarization.

Equation (1) is solved by using the fixed-step fourth-order Runge-Kutta technique with $dt = 0.05$ a.u. The molecular orientation is defined by Euler angles (α, β, γ) . Since γ is needless for a diatomic molecule and it has been proved that α almost has no influence on excitation dynamics, $\beta = [0, \pi]$ is the only useful parameter in this model and $d\beta = \pi/36$ is used. The initial condition in simulations is $\rho(\beta, t = 0) = 0$. The final population distribution is obtained via the space averaging as follows:

$$n_v^M = \frac{\int_0^\pi \rho_{vv}^{MM}(\beta, t_{\text{end}}) \sin\beta d\beta}{\int_0^\pi \sin\beta d\beta}. \quad (3)$$

Population inversion responsible for 391- and 428-nm transitions is extracted by $P_{391} = n_0^B - n_0^X$ and $P_{428} = n_0^B - n_1^X$, respectively. The simulation convergence was tested using more vibrational levels, finer angular resolution, smaller time steps, and the adaptive-step technique, whereas almost identical results were obtained.

IV. RESULTS AND DISCUSSION

The typical spectra of N_2^+ lasing radiation pumped by the 900- and 980-nm lasers are displayed in Figs. 1(c) and 1(d). It can be clearly observed that the seed pulses are significantly amplified when they are tuned to 391 and 428 nm, producing strong N_2^+ lasing radiations at the two wavelengths. As illustrated in Fig. 1(b), the 391- and 428-nm lasing radiation corresponds to the transi-

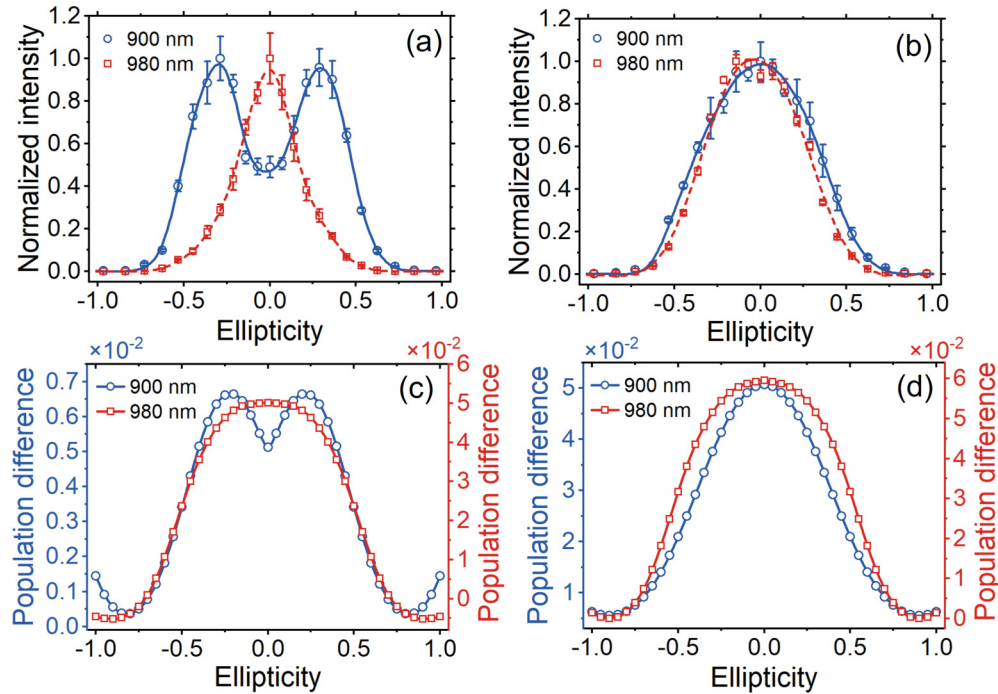


FIG. 2. The measured (a) 391-nm and (b) 428-nm lasing intensity as a function of the ellipticity of the pump laser. Experimental data are fitted to guide the eyes. The calculated population differences (c) P_{391} and (d) P_{428} as a function of ellipticity. The laser intensity adopted in the simulation is $2.3 \times 10^{14} \text{ W/cm}^2$, and the final population differences are averaged over the polar angles.

tion $B(v''=0) - X(v=0)$ and $B(v''=0) - X(v=1)$, respectively. It should be noted that the N_2^+ lasing generated with the seed pulses is more than one order of magnitude stronger than that with the pump alone (not shown), indicating that the seed amplification plays a dominant contribution here. Although the focused intensities of 900- and 980-nm laser pulses were kept nearly the same, the N_2^+ lasing pumped by 980 nm is much stronger compared with the 900-nm pumping, which is attributed to the three-photon resonance of dressed ionic states with the laser field and will be elaborated on later.

In addition, we examined the gain dynamics of N_2^+ lasing at the two pump wavelengths, and obtained similar results to that in the 800-nm pumping case [11, 12]. We also compared the evolutions of the lasing signal with the delay at different pressures. The results show that the gain lifetime decreases with the increasing gas pressure. While measuring the ellipticity dependence of N_2^+ lasing, we fixed the delay at which the strongest lasing radiation is generated. Similar gain dynamics and the fixed delay at different pump wavelengths ensure that the influence of gain dynamics on the ellipticity dependence is negligible.

Figures 2(a) and 2(b) illustrate the dependence of the amplified lasing signals at 391 and 428 nm on the ellipticity of the two pump lasers, respectively. For the 900-nm pumping case (blue circles), the 391-nm lasing signal increases first and then decreases as the pump laser varies from linear to circular polarization. The strongest lasing radiation occurs at the ellipticity of ~ 0.3 . Such ellipticity dependence is in good agreement with the results pumped by 800 nm [29–33]. However, when pumped by the 980-nm laser (red squares), the 391-nm lasing signal decays monotonically with the increasing ellipticity. In comparison, the 428-nm lasing radiation

shows totally different behaviors. As shown in Fig. 2(b), the 428-nm lasing intensity reaches the maximum with the linear polarization laser for both the pumping cases. The comparative results indicate that the ellipticity dependence of the 391-nm lasing is sensitive to the pump wavelength, while the ellipticity dependence of the 428-nm lasing is robust to the variation of the driver wavelength. No obvious amplification is observed when the ellipticity exceeds 0.75 in all cases, which could be attributed to the decrease of the peak electric field strength.

Figures 2(c) and 2(d) illustrate the calculated population differences P_{391} and P_{428} as a function of the laser ellipticity, respectively. As known, the population difference determines by and large the optical gain and the lasing intensity. Therefore, the numerical simulation will help us clarify the physical origin underlying above observation. For the 900-nm pumping case, the ellipticity dependence of P_{391} shows a double-peak structure, and two peaks locate around the ellipticities of ± 0.25 . It is almost consistent with the experimental data in Fig. 2(a). However, in the 980-nm pumping case, the ellipticity dependence of P_{391} shows a bell-shaped shape, as indicated by the red squares. The population inversion reaches the maximum with the linear polarization pulse while it shows negative values near the circular polarization. Nevertheless, the 428-nm lasing signal produced by the two pump wavelengths displays a unimodal structure as the ellipticity varies, as shown in Fig. 2(d). Those theoretical results almost reproduce the experimental observation, suggesting that the population inversion is a dominant mechanism for these N_2^+ lasing radiations in this experiment. We speculate that distinct population dynamics occurs at 900- and 980-nm pump laser wavelengths since they exhibit different polarization-modulated behaviors.

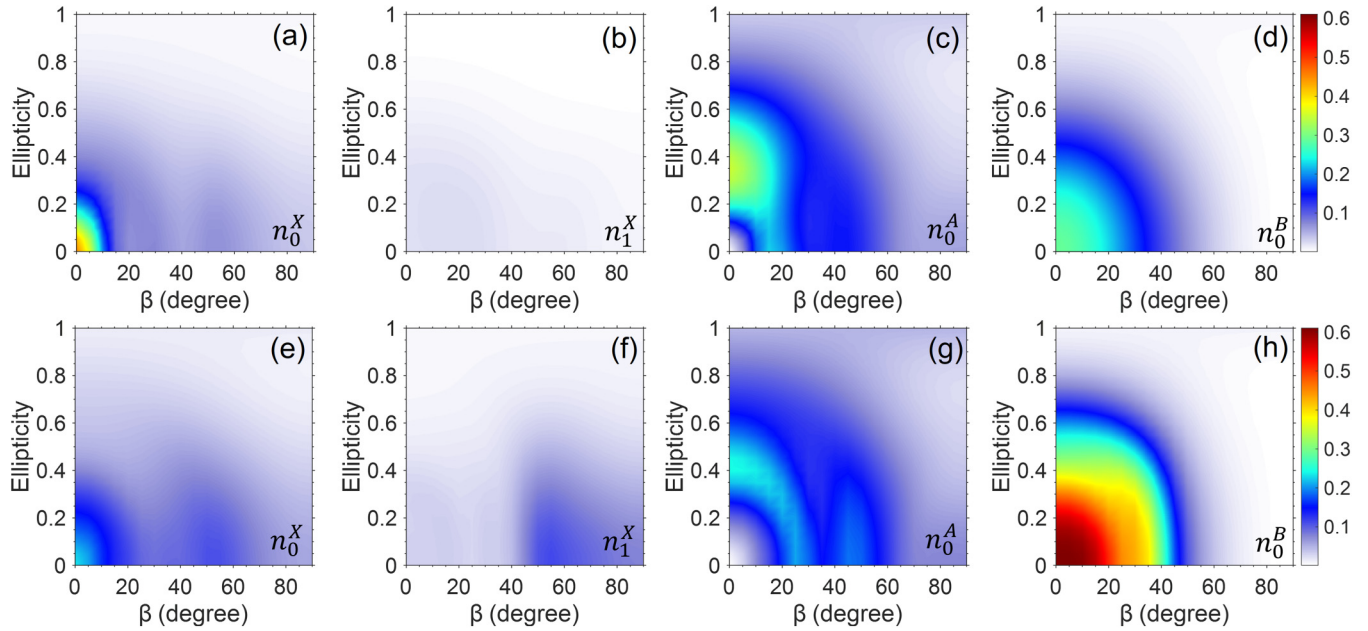


FIG. 3. The calculated vibration-resolved population as functions of the angle β and ellipticity pumped by (a)–(d) 900-nm and (e)–(h) 980-nm lasers.

To reveal the excitation mechanism in N_2^+ , we focus on the final vibration-resolved population distribution on the primary four states, i.e., $X(v = 0, 1)$, $A(v' = 0)$, and $B(v'' = 0)$, in two-parameter space of the laser ellipticity and the polar angle β , as shown in Figs. 3(a)–3(h). The top and bottom panels present the results with the 900- and 980-nm pump lasers, respectively. From the simulation results, we can clearly see that the population on the four states exhibits different angle and ellipticity dependencies. The populations on the $X(v = 0)$ and $B(v'' = 0)$ levels mainly locate in the region of small polar angles and quasilinear polarization. In the case of 900-nm pumping, the population on the $X(v = 0)$ level shows a narrower distribution than that on the $B(v'' = 0)$ level, but it has a larger probability when the ellipticity and angle are close to zero. As a result, the population difference between the two states shows a hole around the origin of coordinates, as shown in Fig. 4(b). Thus, a double-peak structure in Fig. 2(c) is obtained by averaging over the polar angle and taking positive and negative ellipticities into account. When the pump laser wavelength is switched to 980 nm, the $B(v'' = 0)$ population increases significantly and the $X(v = 0)$ population decreases accordingly. It indicates that the population transfer from $X(v = 0)$ to $B(v'' = 0)$ states becomes more efficient at this pump wavelength. Due to a wider and larger population on the $B(v'' = 0)$ level compared to the $X(v = 0)$ level, the population inversion between the two states produced by the 980-nm laser has a maximum around the origin, as shown in Fig. 4(e), leading to a bell-shaped structure in Fig. 2(c).

Moreover, the population on the $A(v' = 0)$ state shows an arc-shaped distribution as the polar angle and ellipticity change, as shown in Figs. 3(c) and 3(g). Actually, the $A(v' = 0)$ population primarily originates from the photoexcitation from the ground state $X(v = 0)$. Thus, the arc-shaped distribution can be attributed to the fact that the condition of $\xi \neq 0$ and $\beta \neq 0$ is beneficial to the perpendicular transition

between the two states. It is noteworthy that the $A(v' = 0)$ state has a higher population in the 900-nm pumping case as compared to the 980-nm case, especially when the ellipticity falls in the range 0.2–0.6. Since there are only two transition channels among the three electronic states of N_2^+ , namely, X - A and X - B , the efficient population transfer from $X(v = 0)$ to $A(v' = 0)$ causes the substantial decrease of the population on the $X(v = 0)$ level, facilitating the population inversion between $B(v'' = 0)$ and $X(v = 0)$. Therefore, the ellipticity dependence of the 391-nm lasing pumped by the 900-nm laser reflects the critical role of the intermediate A state as a reservoir. The population inversion mechanism is similar to the 800-nm pumping case [29–33], thus similar ellipticity dependence is observed here. In contrast, although the $A(v' = 0)$ population also shows the arc-shaped distribution in the 980-nm pumping case, the $B(v'' = 0)$ population is much higher than that of $A(v' = 0)$ state. In this case, the population transfer from $X(v = 0)$ to $B(v'' = 0)$ plays a dominant role in the final population inversion, while the contribution of A state almost can be ignored. Since the electronic transition from X to B states is parallel transition, it is more efficient in the linear polarization. As a result, the 391-nm lasing driven by the 980-nm laser prefers the linear polarization pumping.

Based on these simulation results, we claim that the 900-nm laser field is beneficial for the transition from $X(v = 0)$ to $A(v' = 0)$ levels, while the 980-nm laser favors the transition from $X(v = 0)$ to $B(v'' = 0)$ levels. As is known, the former is a typical one-photon resonance process, which leads to the population inversion between $B(v'' = 0)$ and $X(v = 0)$ states via the $A(v' = 0)$ state as a reservoir. In the 980-nm pumping case, the high population on the $B(v'' = 0)$ state is the result of three-photon resonant excitation, as discussed in the recent study [34]. The photoexcitation processes in the two pumping cases are shown in Fig. 1(b). It is noteworthy that both one-photon and three-photon resonances occur here with

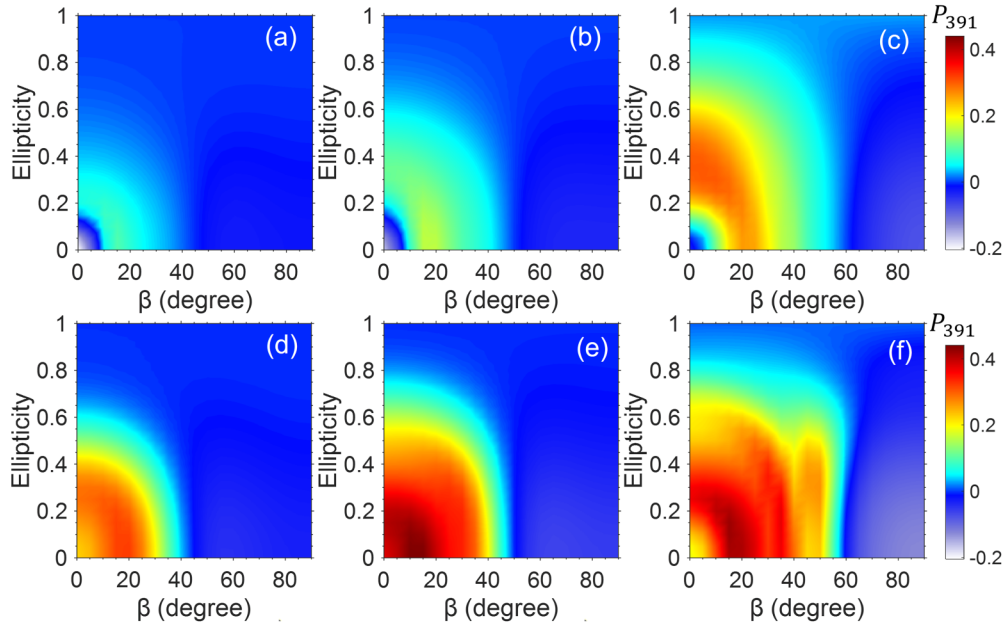


FIG. 4. The calculated population difference P_{391} as functions of the angle β and ellipticity for (a)–(c) 900-nm and (d)–(f) 980-nm pumping cases at three pumping intensities: (a),(d) $2 \times 10^{14} \text{W/cm}^2$; (b),(e) $2.3 \times 10^{14} \text{W/cm}^2$; (c),(f) $3 \times 10^{14} \text{W/cm}^2$.

the assistance of the ac Stark effect. As shown in Fig. 1(b), when the ions are exposed in a strong laser field, their electronic states will shift with the evolution of the pump laser field, resulting in the instantaneous change of the transition energy. In the 980-nm pumping case, the three-photon resonance channel is switched on within the laser field. After the laser field finishes, the lasing radiation occurs via the field-free transition. In the 900-nm pumping case, the one-photon resonance is triggered, which facilitates the population transfer from $X(\nu = 0)$ to $A(\nu' = 0)$ states. The difference in the excitation channel results in different ellipticity dependences

of the 391-nm lasing radiation, while the choice of excitation channel critically depends on the pump laser wavelength.

Figure 4 shows the angle- and ellipticity-dependent population difference P_{391} at three pump laser intensities. For the 900-nm pumping case, the population difference always shows arc-shaped distribution at all intensities. However, for the 980-nm pumping case, the large population difference appears in the region of small β angles and small ellipticities at the laser intensities of $2 \times 10^{14} \text{W/cm}^2$ and $2.3 \times 10^{14} \text{W/cm}^2$. When the laser intensity reaches $3 \times 10^{14} \text{W/cm}^2$, the population difference also exhibits the arc-shaped distribution,

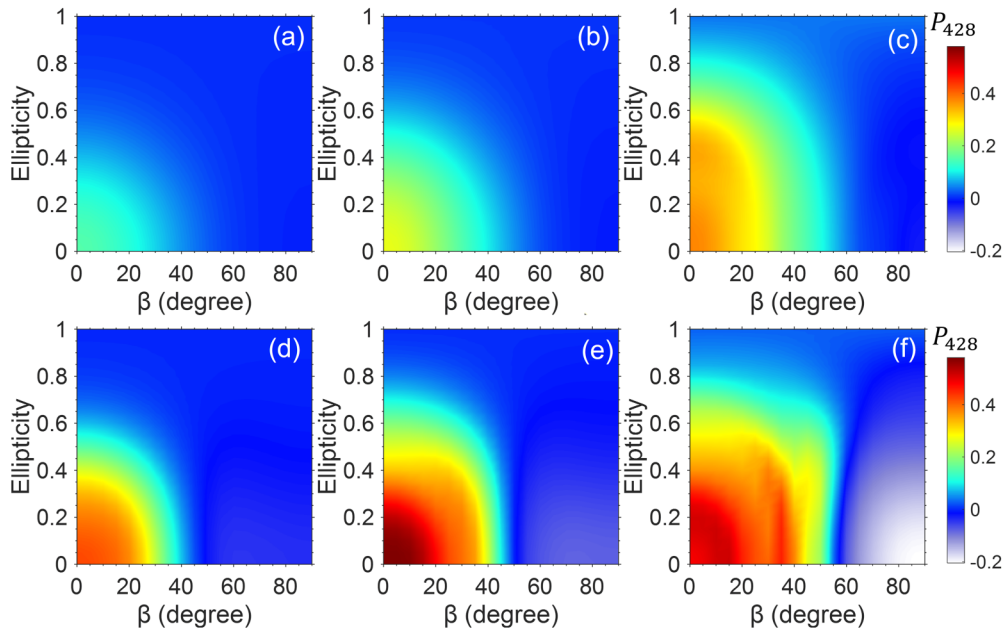


FIG. 5. The calculated population difference P_{428} as functions of the angle β and ellipticity for (a)–(c) 900-nm and (d)–(f) 980-nm pumping cases at three pumping intensities: (a),(d) $2 \times 10^{14} \text{W/cm}^2$; (b),(e) $2.3 \times 10^{14} \text{W/cm}^2$; (c),(f) $3 \times 10^{14} \text{W/cm}^2$.

indicating that the $A(\nu' = 0)$ state becomes important in this case. The dynamic three-photon resonance assisted by the ac Stark effect only takes place in a certain intensity range, beyond which the three-photon resonance becomes less efficient owing to the energy detuning. In this case, the population inversion will need the assistance of one-photon excitation.

Compared with the 391-nm lasing, the ellipticity dependence of the 428-nm lasing is totally different. As shown in Fig. 3, the population on the $X(\nu = 1)$ level is much lower than other three levels for two reasons as follows. On the one hand, the ionization injection probability is very low from the neutral nitrogen molecule to the $X(\nu = 1)$ level of N_2^+ due to the Franck-Condon factor as low as 0.0779 [36]. On the other hand, since the transition between different vibrational levels of X state is forbidden, the population on the $X(\nu = 0)$ level is hardly transferred to the $X(\nu = 1)$ level. Since the $X(\nu = 1)$ population is almost negligible, the strength of the 428-nm lasing radiation mainly depends on the population of the upper level $B(\nu'' = 0)$. The $B(\nu'' = 0)$ population mainly originates from the photoexcitation from the X state of N_2^+ or the photoionization from the ground state of the neutral nitrogen molecule. For both channels, the $B(\nu'' = 0)$ population primarily locates around the small angles and quasilinear polarization. As a result, the population difference between $B(\nu'' = 0)$ and $X(\nu = 1)$ levels (i.e., P_{428}) shows similar distribution at various intensities for the two pumping cases, as shown in Figs. 5(a)–5(f).

V. CONCLUSION

In summary, we compared polarization-modulated behaviors of N_2^+ lasing in 900- and 980-nm pumping cases by combined experimental and theoretical studies. For the 391-nm lasing signal, the ellipticity dependence shows a distinct difference at the two pump wavelengths, which is attributed to different excitation channels. Unlike the 391-nm lasing radiation, the 428-nm signal displays a unimodal structure in two pumping cases, due to the low population on the $X(\nu = 1)$ level. The current study uncovers the sensitivity of population inversion created in the multilevel N_2^+ system on the laser parameters, which in turn allows us to enhance and modulate N_2^+ lasing by optimizing the laser wavelength and polarization states.

ACKNOWLEDGMENTS

This work was supported by the National Natural Science Foundation of China (Grants No. 12034013, No. 12274428, No. 12204308, and No. 12374320), Youth Innovation Promotion Association of Chinese Academy of Sciences (CAS) (Grant No. Y2022072), CAS Project for Young Scientists in Basic Research (Grant No. YSBR-042), and Natural Science Foundation of Shanghai (Grants No. 22ZR1481600, No. 23ZR1471700, and No. 22ZR1444100). The authors are grateful to Dr. S. Xue for the helpful and enlightening discussions.

-
- [1] L. V. Keldysh, Ionization in the field of a strong electromagnetic wave, *Sov. Phys. JETP* **20**, 1307 (1965).
- [2] A. Gold and H. B. Bebb, Theory of multiphoton ionization, *Phys. Rev. Lett.* **14**, 60 (1965).
- [3] X. M. Tong, Z. X. Zhao, and C. D. Lin, Theory of molecular tunneling ionization, *Phys. Rev. A* **66**, 033402 (2002).
- [4] J. Yao, B. Zeng, H. Xu, G. Li, W. Chu, J. Ni, H. Zhang, S. L. Chin, Y. Cheng, and Z. Xu, High-brightness switchable multiwavelength remote laser in air, *Phys. Rev. A* **84**, 051802(R) (2011).
- [5] J. Yao, W. Chu, Z. Liu, J. Chen, B. Xu, and Y. Cheng, An anatomy of strong-field ionization-induced air lasing, *Appl. Phys. B: Lasers Opt.* **124**, 73 (2018).
- [6] P. Polynkin and Y. Cheng, *Air Lasing* (Springer, Switzerland, 2018).
- [7] J. Yao, G. Li, C. Jing, B. Zeng, W. Chu, J. Ni, H. Zhang, H. Xie, C. Zhang, H. Li, H. Xu, S. L. Chin, Y. Cheng, and Z. Xu, Remote creation of coherent emissions in air with two-color ultrafast laser pulses, *New J. Phys.* **15**, 023046 (2013).
- [8] J. Yao, S. Jiang, W. Chu, B. Zeng, C. Wu, R. Lu, Z. Li, H. Xie, G. Li, C. Yu, Z. Wang, H. Jiang, Q. Gong, and Y. Cheng, Population redistribution among multiple electronic states of molecular nitrogen ions in strong laser fields, *Phys. Rev. Lett.* **116**, 143007 (2016).
- [9] H. Xu, E. Lötstedt, A. Iwasaki, and K. Yamanouchi, Sub-10-fs population inversion in N_2^+ in air lasing through multiple state coupling, *Nat. Commun.* **6**, 8347 (2015).
- [10] M. Britton, M. Lytova, P. Laferrrière, P. Peng, F. Morales, D. H. Ko, M. Richter, P. Polynkin, D. M. Villeneuve, C. Zhang, M. Ivanov, M. Spanner, L. Arissian, and P. B. Corkum, Short- and long-term gain dynamics in N_2^+ air lasing, *Phys. Rev. A* **100**, 013406 (2019).
- [11] H. Zhang, C. Jing, J. Yao, G. Li, B. Zeng, W. Chu, J. Ni, H. Xie, H. Xu, S. L. Chin, K. Yamanouchi, Y. Cheng, and Z. Xu, Rotational coherence encoded in an “air-laser” spectrum of nitrogen molecular ions in an intense laser field, *Phys. Rev. X* **3**, 041009 (2013).
- [12] W. Zheng, Z. Miao, L. Zhang, Y. Wang, C. Dai, A. Zhang, H. Jiang, Q. Gong, and C. Wu, Enhanced coherent emission from ionized nitrogen molecules by femtosecond laser pulses, *J. Phys. Chem. Lett.* **10**, 6598 (2019).
- [13] T. Ando, E. Lötstedt, A. Iwasaki, H. Li, Y. Fu, S. Wang, H. Xu, and K. Yamanouchi, Rotational, vibrational, and electronic modulations in N_2^+ lasing at 391 nm: Evidence of coherent $B^2\Sigma_u^+ - X^2\Sigma_g^+ - A^2\Pi_u$ coupling, *Phys. Rev. Lett.* **123**, 203201 (2019).
- [14] Q. Zhang, H. Xie, G. Li, X. Wang, H. Lei, J. Zhao, Z. Chen, J. Yao, Y. Cheng, and Z. Zhao, Sub-cycle coherent control of ionic dynamics via transient ionization injection, *Commun. Phys.* **3**, 50 (2020).
- [15] Y. Zhang, E. Lötstedt, and K. Yamanouchi, Effects of ionization timing for off-resonant population transfer by positionization excitation in N_2^+ , *Phys. Rev. A* **106**, 063109 (2022).
- [16] M. Britton, M. Lytova, D. H. Ko, A. Alqasem, P. Peng, D. M. Villeneuve, C. Zhang, L. Arissian, and P. B. Corkum, Control of N_2^+ air lasing, *Phys. Rev. A* **102**, 053110 (2020).

- [17] A. Azarm, P. Corkum, and P. Polynkin, Optical gain in rotationally excited nitrogen molecular ions, *Phys. Rev. A* **96**, 051401(R) (2017).
- [18] M. Richter, M. Lytova, F. Morales, S. Haessler, O. Smirnova, M. Spanner, and M. Ivanov, Rotational quantum beat lasing without inversion, *Optica* **7**, 586 (2020).
- [19] A. Mysyrowicz, R. Danylo, A. Houard, V. Tikhonchuk, X. Zhang, Z. Fan, Q. Liang, S. Zhuang, L. Yuan, and Y. Liu, Lasing without population inversion in N_2^+ , *APL Photonics* **4**, 110807 (2019).
- [20] Y. Liu, P. Ding, G. Lambert, A. Houard, V. Tikhonchuk, and A. Mysyrowicz, Recollision-induced superradiance of ionized nitrogen molecules, *Phys. Rev. Lett.* **115**, 133203 (2015).
- [21] Y. Liu, P. Ding, N. Ibrakovic, S. Bengtsson, S. Chen, R. Danylo, E. R. Simpson, E. W. Larsen, X. Zhang, Z. Fan, A. Houard, J. Mauritsson, A. L'Huillier, C. L. Arnold, S. Zhuang, V. Tikhonchuk, and A. Mysyrowicz, Unexpected sensitivity of nitrogen ions superradiant emission on pump laser wavelength and duration, *Phys. Rev. Lett.* **119**, 203205 (2017).
- [22] H. Li, M. Hou, H. Zang, Y. Fu, E. Lötstedt, T. Ando, A. Iwasaki, K. Yamanouchi, and H. Xu, Significant enhancement of N_2^+ lasing by polarization-modulated ultrashort laser pulses, *Phys. Rev. Lett.* **122**, 013202 (2019).
- [23] J. Chen, J. Yao, H. Zhang, Z. Liu, B. Xu, W. Chu, L. Qiao, Z. Wang, J. Fatome, O. Faucher, C. Wu, and Y. Cheng, Electronic-coherence-mediated molecular nitrogen-ion lasing in a strong laser field, *Phys. Rev. A* **100**, 031402(R) (2019).
- [24] H. Li, E. Lötstedt, H. Li, Y. Zhou, N. Dong, L. Deng, P. Lu, T. Ando, A. Iwasaki, Y. Fu, S. Wang, J. Wu, K. Yamanouchi, and H. Xu, Giant enhancement of air lasing by complete population inversion in N_2^+ , *Phys. Rev. Lett.* **125**, 053201 (2020).
- [25] A. Zhang, M. Lei, J. Gao, C. Wu, Q. Gong, and H. Jiang, Subfemtosecond-resolved modulation of superfluorescence from ionized nitrogen molecules by 800-nm femtosecond laser pulses, *Opt. Express* **27**, 14922 (2019).
- [26] A. Zhang, Q. Liang, M. Lei, L. Yuan, Y. Liu, Z. Fan, X. Zhang, S. Zhuang, C. Wu, Q. Gong, and H. Jiang, Coherent modulation of superradiance from nitrogen ions pumped with femtosecond pulses, *Opt. Express* **27**, 12638 (2019).
- [27] J. Yao, L. Wang, J. Chen, Y. Wan, Z. Zhang, F. Zhang, L. Qiao, S. Yu, B. Fu, Z. Zhao, C. Wu, V. V. Yakovlev, L. Yuan, X. Chen, and Y. Cheng, Photon retention in coherently excited nitrogen ions, *Sci. Bull.* **66**, 1511 (2021).
- [28] H. Lei, J. Yao, J. Zhao, H. Xie, F. Zhang, H. Zhang, N. Zhang, G. Li, Q. Zhang, X. Wang, Y. Yang, L. Yuan, Y. Cheng, and Z. Zhao, Ultraviolet supercontinuum generation driven by ionic coherence in a strong laser field, *Nat. Commun.* **13**, 4080 (2022).
- [29] H. Zhang, C. Jing, G. Li, H. Xie, J. Yao, B. Zeng, W. Chu, J. Ni, H. Xu, and Y. Cheng, Abnormal dependence of strong-field-ionization-induced nitrogen lasing on polarization ellipticity of the driving field, *Phys. Rev. A* **88**, 063417 (2013).
- [30] M. Britton, P. Laferrière, D. H. Ko, Z. Li, F. Kong, G. Brown, A. Naumov, C. Zhang, L. Arissian, and P. B. Corkum, Testing the role of recollision in N_2^+ air lasing, *Phys. Rev. Lett.* **120**, 133208 (2018).
- [31] Y. Fu, E. Lötstedt, H. Li, S. Wang, D. Yao, T. Ando, A. Iwasaki, F. H. M. Faisal, K. Yamanouchi, and H. Xu, Optimization of N_2^+ lasing through population depletion in the $X^2\Sigma_g^+$ state using elliptically modulated ultrashort intense laser fields, *Phys. Rev. Res.* **2**, 012007(R) (2020).
- [32] Y. Wan, B. Xu, J. Yao, J. Chen, Z. Liu, F. Zhang, W. Chu, and Y. Cheng, Polarization ellipticity dependence of N_2^+ air lasing: The role of coupling between the ground state and a photo-excited intermediate state, *J. Opt. Soc. Am. B* **36**, G57 (2019).
- [33] Z. Zhu, S. Xue, Y. Zhang, Y. Zhang, R. Yang, S. Sun, Z. Liu, P. Ding, and B. Hu, Influence of polarization ellipticity on N_2^+ lasing in a strong laser field, *Phys. Rev. A* **108**, 013111 (2023).
- [34] Y. Chen, H. Lei, Q. Wang, H. Xie, H. Zhang, X. Lu, N. Zhang, S. Huang, Y. Wu, J. Liu, Q. Zhang, Y. Liu, Z. Zhao, J. Zhao, and J. Yao, Enhanced population on ionic excited states by synchronized ionization and multiphoton resonance, [arXiv:2307.00958](https://arxiv.org/abs/2307.00958).
- [35] V. T. Tikhonchuk, Y. Liu, R. Danylo, A. Houard, and A. Mysyrowicz, Theory of femtosecond strong field ion excitation and subsequent lasing in N_2^+ , *New J. Phys.* **23**, 023035 (2021).
- [36] F. R. Gilmore, R. R. Laher, and P. J. Espy, Franck-Condon factors, r -centroids, electronic transition moments, and Einstein coefficients for many nitrogen and oxygen band systems, *J. Phys. Chem. Ref. Data* **21**, 1005 (1992).
- [37] S.-F. Zhao, C. Jin, A.-T. Le, T. F. Jiang, and C. D. Lin, Determination of structure parameters in strong-field tunneling ionization theory of molecules, *Phys. Rev. A* **81**, 033423 (2010).